

Article

Experimental Investigation of the Mechanical Behaviors of Grouted Sand with UF-OA Grouts

Yuhao Jin ^{1,2} , Lijun Han ^{1,2}, Qingbin Meng ², Dan Ma ³, Guansheng Han ^{2,*}, Furong Gao ¹ and Shuai Wang ²

¹ School of Mechanics and Civil Engineering, China University of Mining and Technology, Xuzhou 221116, China; jinyuhao@cumt.edu.cn (Y.J.); hanlj@cumt.edu.cn (L.H.); furong_gao@126.com (F.G.)

² State Key Laboratory for Geomechanics and Deep Underground Engineering, China University of Mining and Technology, Xuzhou 221116, China; mqb1985@cumt.edu.cn (Q.M.); shwzzh023@163.com (S.W.)

³ School of Resources & Safety Engineering, Central South University, Changsha 410083, China; dan.ma@csu.edu.cn

* Correspondence: Han_GS@cumt.edu.cn; Tel.: +86-15162181307

Received: 29 March 2018; Accepted: 15 April 2018; Published: 19 April 2018



Abstract: A detailed understanding of the engineering properties for grouted sand is a key concern in foundation engineering projects containing sand layers. In this research, experiments of grouting with various grain sizes of sand specimens using a new type of improved chemical material-urea formaldehyde resin mixed with oxalate curing agent (UF-OA), which has rarely been used as grout in the reinforcement of soft foundations, were conducted on the basis of a self-developed grouting test system. After grouting tests, the effects on the mechanical behaviors of grouted sand specimens were investigated through uniaxial compression tests considering the grain size, the presence or absence of initial water in sand, and the curing time for grouted sand. Experimental results show that with the increase in the grain size and the presence of initial water in the sand specimen, the values of uniaxial compressive strength (UCS) and elastic moduli (E) of the grouted specimens decreased obviously, indicating that the increase of grain size and the presence of initial water have negative impacts on the mechanical behaviors of grouted sand; the peak strains (ϵ_c) were almost unchanged after 14 days of curing; no brittle failure behavior occurred in the grouted specimens, and desirable ductile failure characteristics were distinct after uniaxial compression. These mechanical behaviors were significantly improved after 14 days of curing. The micro-structural properties obtained by scanning electron microscopy (SEM) of the finer grouted sand indicate preferable filling performance to some extent, thereby validating the macroscopic mechanical behaviors.

Keywords: chemical grouts; grain size of sand; initial water contained in sand; grouted sand; macroscopic mechanical behaviors; microstructure characteristics; ductile failure

1. Introduction

Chemical grouting is a well-known reinforcement method in geotechnical engineering, and is used to reduce the permeability and increase the mechanical strength of the soil and rock mass. Grout flowing through the soil and fracture network within the rock mass are similar to the flow of fluid (or gas) through rock fracture networks [1–4]. Chemical grouts can penetrate tiny pores in some dense but weak sand layers, where conventional Portland cement grouts are likely to fail [5,6], although cement-based grouts are more widely used [7–9]. In recent years, many experimental results on the mechanical behaviors of grouted sand using chemical grouts have been achieved. For example, Anagnostopoulos, Papaliangas [10] investigated the mechanical behaviors of grouted sand and found that the epoxy resin grouts of low water content caused an increase in strength and a decrease in

water permeability. Xing, Dang [11] conducted experiments to study the mechanical properties of chemically grouted sand and found that the dense polymer film–sand matrix after grouting also led to a significant decrease in water permeability and an increase in mechanical strength. Porcino, Ghionna [12] discussed the mechanical and hydraulic properties of sand injected with mineral-based grouts or silicate solution, and showed that both mechanical strength and initial shear modulus in the mineral-based grouted sand were higher than those of grouted sand using silicate solution. Dayakar, Raman [13] performed an experiment on the influence of cement grouts on the supporting capacity of sandy soil, and demonstrated that the strength of grouted specimens was improved with the increase of the cement content. Some researchers also investigated the strength properties of sodium silicate-grouted soils [14–18], and found that within a certain range, the mechanical strengths of the grouted soils decreased with the increase of water content in different types of grouts.

The above research results mainly focused on the influence of the different chemical and cement grouts (especially the amount of water in the grouts) on the mechanical parameters of the grouted sand; however, no variation of the curing time of grouted sand specimens was considered. Moreover, in terms of the grouting material, the improved chemical material UF-OA (a urea formaldehyde resin mixed with an oxalate curing agent that can be used to accelerate the curing process), characterized by high bonding strength, low production cost, sufficient raw materials and non-polluting nature [19], has rarely been used as grout for reinforcing soft foundations. Furthermore, the impact of the initial water contained in sand is also crucial to the mechanical mechanism, which has yet to be studied in chemical grouted sand up to now. To address these gaps in knowledge, a series of samples were prepared, and studies were conducted:

The gel time, concretion rate, and mechanical and rheological properties of UF-OA grouts with various volume ratios between A and B (A-volume of urea formaldehyde resin, and B-volume of oxalate curing agent) were determined to obtain a suitable volume ratio of A and B in the grouts.

The sand specimens with different grain sizes were prepared (defined as “large-grain sand”, “medium-grain sand” and “small-grain sand”, corresponding to different porosity), and the grouting apparatus was developed specifically for the grouting experiments in the study.

Through the tests of permeation grouting using the UF-OA chemical grouting material, uniaxial compression and scanning electron microscopy (SEM), the mechanical and microscopic characteristics of the grouted sand specimens were obtained, taking into account the different particle size (porosity), the existence (or absence) of the initial water (to facilitate the comparative study of the two, ω_{wc} of 0% and 5% were only selected in the study) in the sand specimens, as well as the different curing times of 3, 7, 14 and 28 days.

2. Experimental Work

2.1. Specimen Preparation

The results of tests of the physical parameters of the sand are shown in Table 1, including grain size, water content, average porosity and mass density. Based on the relative grain size, the sand specimens used in the experiment were divided into three major types (large-grain, medium-grain, and small-grain sand, which can be quantified as the porosity); the specimens were placed in a cylindrical grouting barrel with diameter of 150 mm and height of 200 mm and then subjected to grout injection with UF grouts during the grouting tests.

Table 1. Physical parameters of sand specimens before grouting.

Sand Category Used in the Tests	Grain Size (mm)	Water Content (%)	Average Initial Porosity	Average Mass Density (g/cm ³)
Large-grain	0.5 < d < 0.85	0	34	2.52
		5	30	2.61
Medium-grain	0.25 < d < 0.42	0	36	2.67
		5	32	2.74
Small-grain	0.11 < d < 0.21	0	40	2.72
		5	37	2.80

The parameter acquisition process is briefly described below:

Grain size:

The different grain sizes were gained by using a shaking screen, etc.

Water content:

$$\omega_{WC} = \frac{g_1 - g_2}{g_2} \times 100\% \quad (1)$$

where ω_{wc} refers to the water content of initial sand (before grouting), g_1 and g_2 denote the weight of the specimen with water and the dry specimen, respectively. It is worth noting that the water content in this paper was known (5%), and the amount of water needed to be added was calculated by using this formula in the process of sample making. A high-precision electronic balance and an oven are necessary.

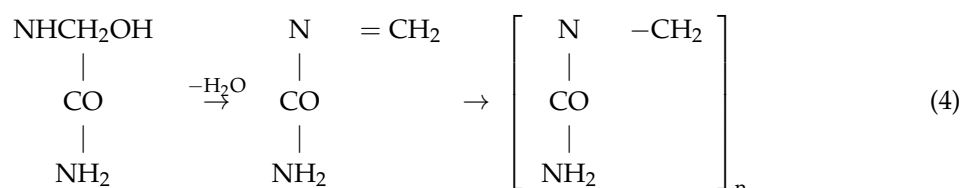
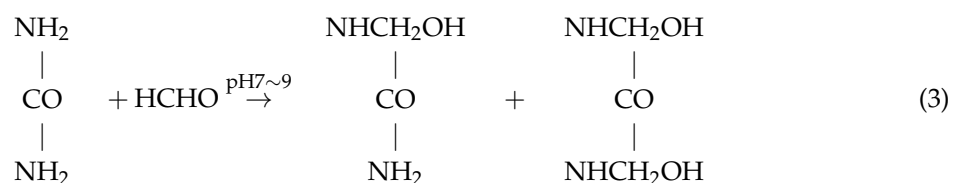
Initial porosity:

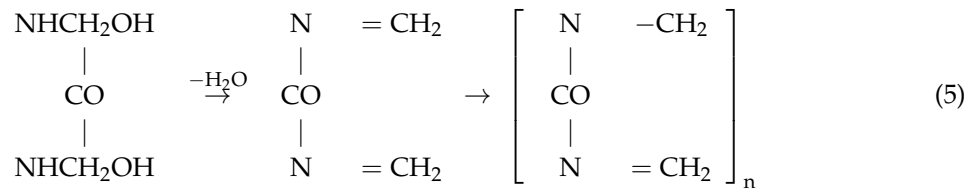
We measured the volume of the material in the natural state V_0 (apparent volume), quality of the material m and density of the material ρ , and then used the formula for porosity expressed as:

$$\phi = \left(1 - \frac{m/V_0}{\rho}\right) \times 100\% \quad (2)$$

2.2. Chemical Reaction of Grout Components

When the urea formaldehyde resin was mixed with the oxalate curing agent to improve the property of the urea formaldehyde resin, the following reactions occurred, as shown in Equations (3)–(5) [20]. According to the reaction equation, in the addition reaction stage (Equation (3)), urea reacts with formaldehyde water, generating hydroxymethyl urea and dihydroxymethyl urea in the case of the weak base. Then, the oxalic acid reacts with the hydroxymethyl urea and dihydroxymethyl urea according to Equations (4) and (5), respectively, to produce acidic solution. In the acidic condition, various polymethylenes are produced to achieve solidification.





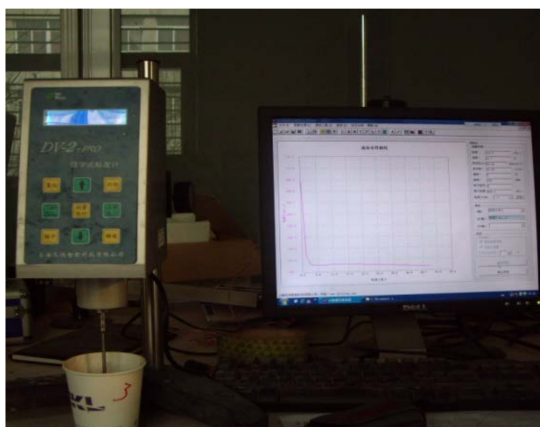
2.3. Properties of UF-OA Grouts

Through a series of physical and mechanical tests, the elastic modulus and Poisson's ratio of the grout gels with different volume ratios were obtained by mechanical test, as shown in Table 2.

Table 2. Elastic modulus and Poisson's ratio of the grout gel with different volume ratios obtained by using uniaxial compressive strength tests.

A:B	4:1	5:1	6:1	7:1
Elastic Modulus (MPa)	120	140	180	220
Poisson's Ratio	0.187	0.211	0.25	0.3

Moreover, the gel time and concretion rate with different volume ratios, viscosity variation with time, UCS variation with different curing time, and the ultimate compressive failure characteristics of the grout gel were determined: the gel time, concretion rate, and viscosity were tested by using a digital viscometer, as shown in Figure 1a. The uniaxial compressive strengths (UCSs) were obtained after the uniaxial compression tests, as displayed in Figure 1b. Figure 1c shows that the gel time and concretion rate both increased as the volume ratio of A and B increased. The values of gel time and concretion rate at A:B of 7 were 330 s and 99.2%, respectively. Similar to the above two parameters, the uniaxial compressive strengths at the same curing time were enhanced with the increasing A:B. In addition, the mechanical strengths also increased with the increase of curing time while keeping A:B unchanged, as shown in Figure 1e. The ultimate compressive failure of the UF-OA grouts, featuring the expansion and vertical splitting fracture of the gel, are as shown in Figure 1f. As shown in Figure 1d, the viscosity of the grouts increased with time but decreased with the increase in A:B. These findings indicated that the UF-OA grouts with an A:B of 7 would have better mechanical characteristics and flow properties than those with other volume ratios. Therefore, UF-OA grouts with a volume ratio of 7 were chosen in this study.



(a)



(b)

Figure 1. Cont.

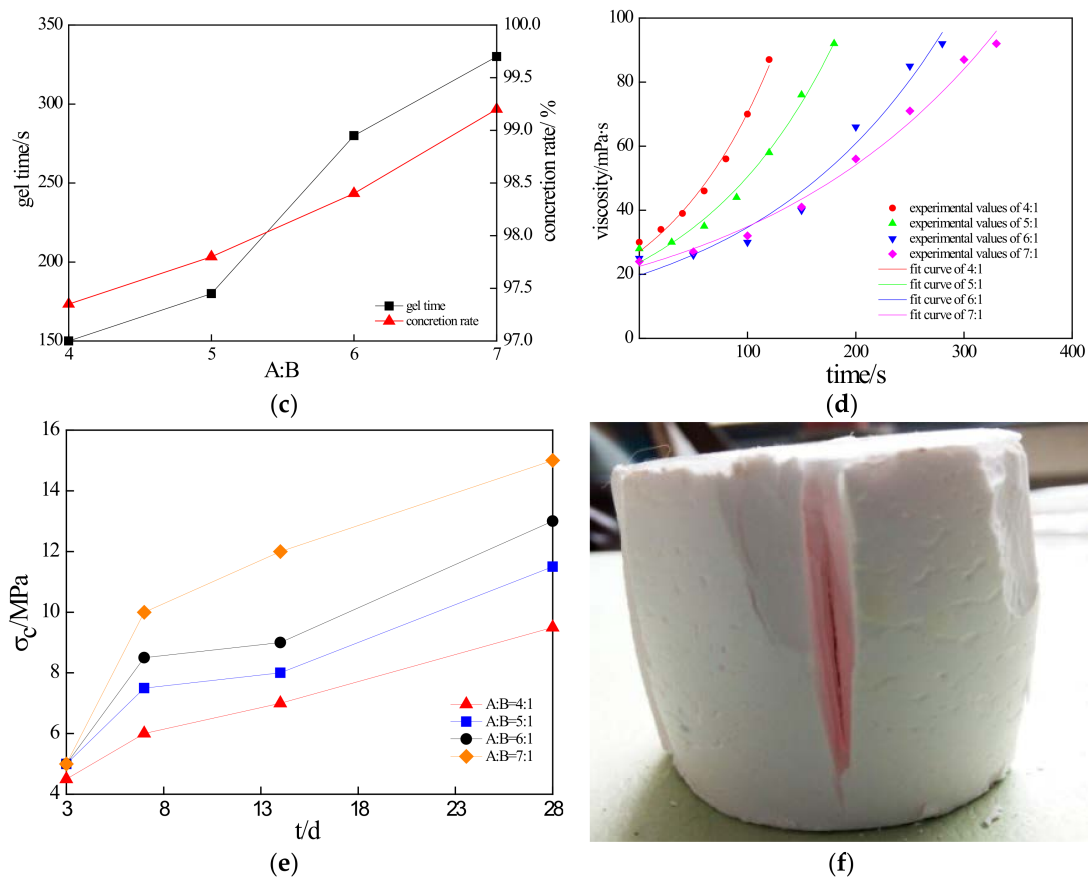


Figure 1. Rheological and mechanical properties of the UF-OA (urea formaldehyde resin mixed with oxalate curing agent) grouts, including (a) the digital viscometer; (b) specimen under compression; (c) gel time and concretion rate with different volume ratios; (d) viscosity variation with time; (e) uniaxial compressive strength (UCS) variation with different curing time; and (f) the ultimate compressive failure characteristics of grout gel.

2.4. Laboratory Procedure

The grouting test was conducted by injecting a measurable quantity of UF grouts into the sand specimen that was placed in the grouting barrel by using the self-designed grouting experimental setup, which is composed of a ground stress simulation system, a grouting test system (the cylindrical grouting barrel is assembled by two pieces of semi-cylindrical barrels for convenience in installation and disassembly), a grouting pressure gauge, a grout transmission system, and a grout supply system, as shown in Figure 2. Note that the testing machine can apply an axial pressure as well as a lateral restraining action (Poisson effect) on the specimen inside the grouting barrel via the load-bearing plate, which can be easily moved up and down in the grouting barrel to represent the ground stress in the real situation (Equation (6)). Moreover, the fixed axial pressure and the lateral restraint in the grouting apparatus can ensure that the porosity remains close to constant during the experiment.

$$\frac{F}{A} = \gamma H, \quad (6)$$

where F and A refer to the axial force provided by the testing machine and the area of load-bearing plate (0.02 m^2), respectively, γ denotes the average unit weight for sand layers (20 kN/m^3), and H is related to the ground depth. Here, H of 10 m was set up in the study, and the corresponding axial force F of 4 kN was calculated.

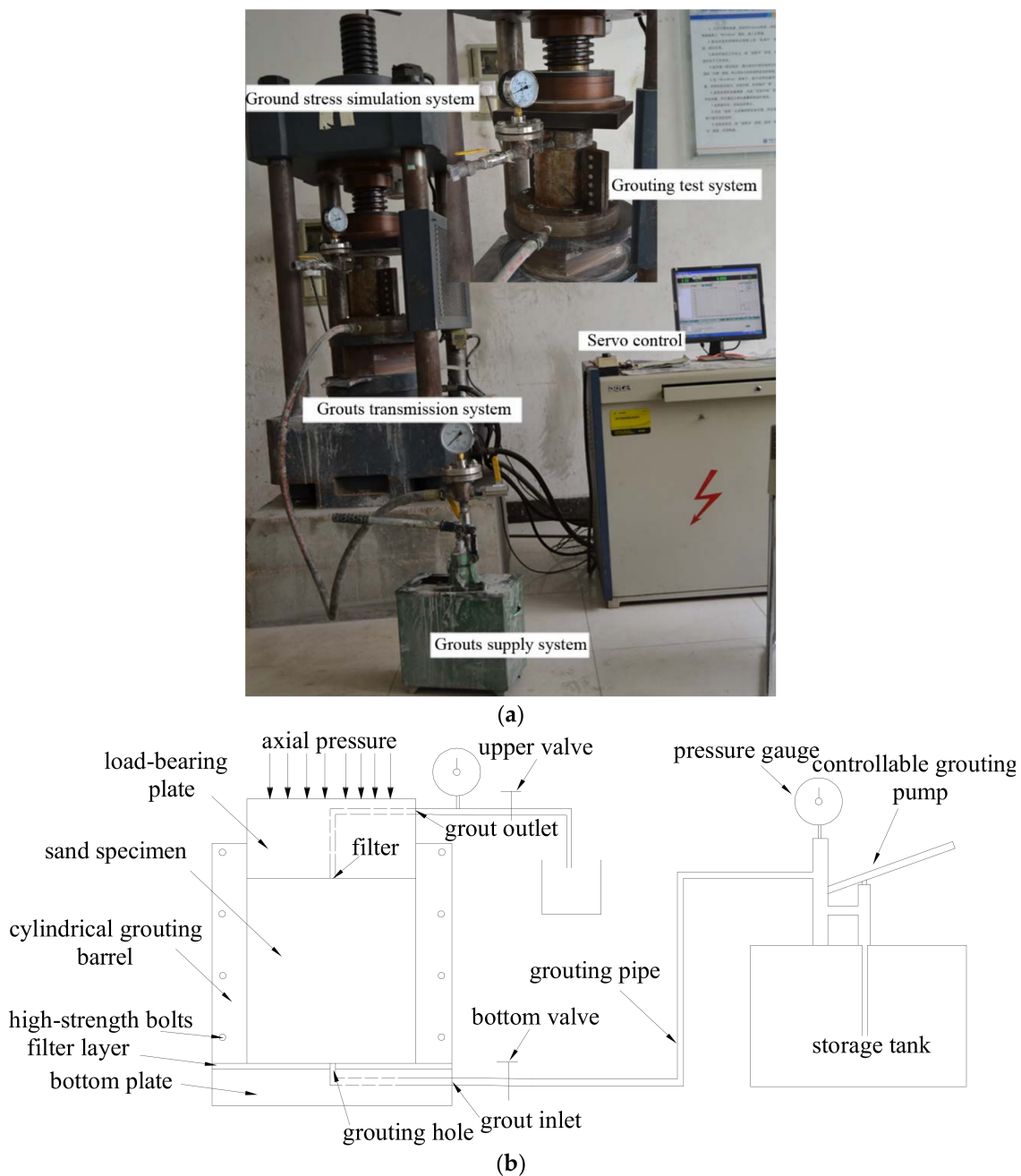


Figure 2. (a) Grouting experimental setup and (b) detailed schematic layout of the grouting test system.

After performing the grouting tests and curing for the designed times (3, 7, 14 and 28 days), referring to the uniaxial compression test standard [21], the grouted standard cylindrical sand specimens with the same height-to-diameter ratio of 2 (100 mm × 50 mm) for different grain size and initial water conditions were extracted from the grouting reinforced body (150 mm × 200 mm) in the grouting barrel, and then these grouted specimens were subjected to uniaxial compression tests using the CMT5305 electronic universal testing machine at a loading rate of 3×10^{-3} mm per second. Finally, after 28 days of curing, the microstructure scanning tests for the grouted specimens not subjected to the uniaxial compression tests were conducted using SEM.

To prevent the hydrofracturing of sand specimens from occurring, the grouting pressure during the grouting experiments must be maintained at a lower level (while the grouting pressures in the “hydrofracturing grouting” are larger and have larger serrated changes during the grouting

experiments) using a hand grouting pump (which allows for easy adjustment of the grouting pressure) and a pressure gauge to ensure the penetration of the grouts in the sand samples. Note that each of the reported values for mechanical parameters in this study represent the average value of three specimens.

3. Results

3.1. Macroscopic Mechanical Parameters

To study the differences in mechanical behaviors among the multiple grouted specimens of different grain size and initial water conditions at 3, 7, 14 and 28 days of curing, different axial stress–strain curves of grouted sand specimens after the uniaxial compression tests are shown in Figure 3. Because the grouts in small-grain sand could not be sufficiently hardened in a short time, no corresponding effective experimental results were obtained on the small-grain grouted specimens after 3 days of curing, as shown in Figure 3a. More details are described in the Discussion.

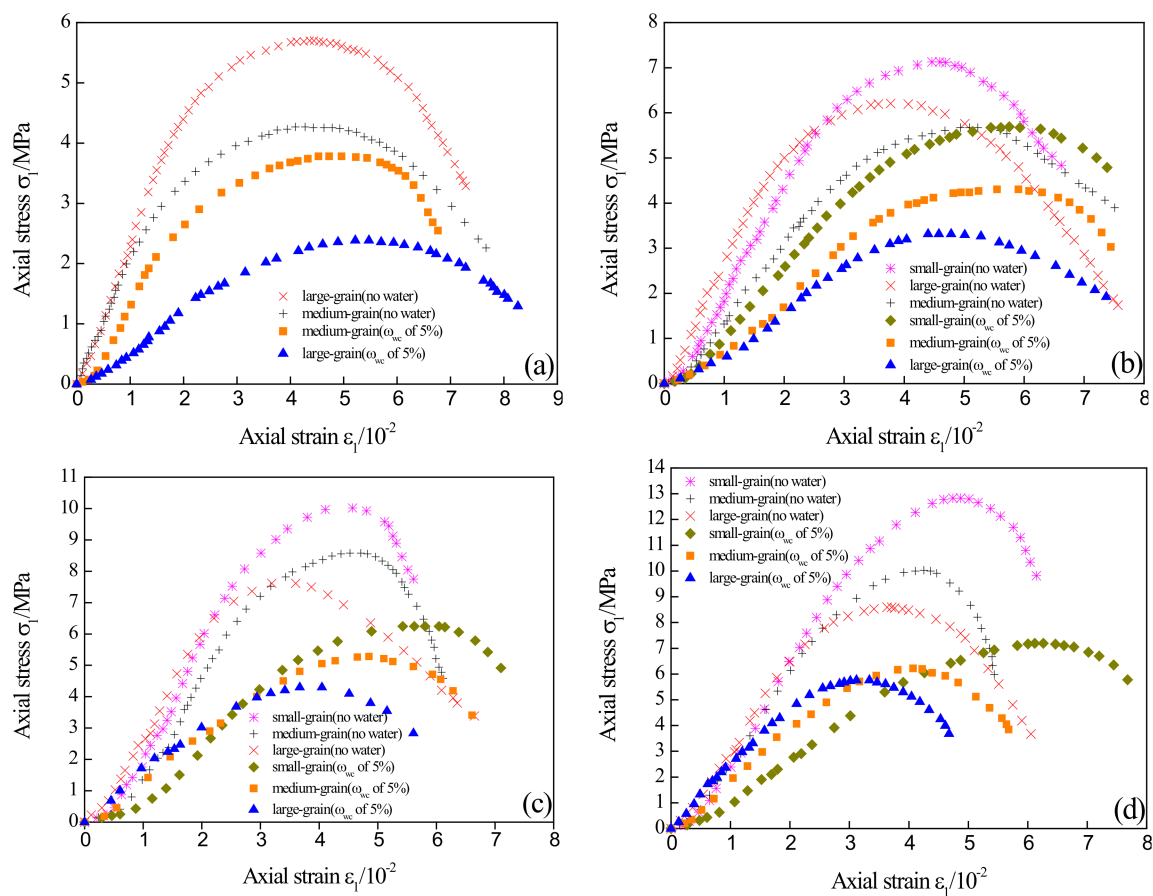


Figure 3. Axial stress–strain curves of representative grouted sand specimens with different grain size and water-contained condition of sand after curing treatment: (a–d) at 3, 7, 14 and 28 days of curing, respectively.

Figures 4 and 5 illustrate the evolution of the different mechanical parameters (namely, uniaxial compressive strength (UCS), elastic modulus (E), and peak axial strain (ϵ_c)) of the grouted sand specimens (see Table 3) with curing time (t) and porosity (φ), respectively. Figure 4a revealed that the average values of UCS for all of the grouted specimens in different grain sizes and initial water content increased distinctly with the increase in curing time (from 3 to 28 days). However, the slopes of curves decreased gradually after 14 days of curing (the slopes were quantified by linear fit, as shown in Figure 4a), this observation indicated that the mechanical behaviors for grouted specimens

after 14 days of curing appeared to obtain satisfactory improvement. From the curing time of 3 (or 7) to 28 days, the average values of UCS of the grouted specimens not containing initial water increased by approximately 80% in the specimens with small grain size, compared to 76% and 51% with medium and large grain size, respectively, indicating that the curing time had positive effects on improving the mechanical characteristics of the sand after grouting, especially for the sand of smaller grain size. The evolution of UCS over curing time in grouted specimens containing initial water was consistent with that of the specimens without initial water. Additionally, as shown in Figure 5a, for the same curing time, the UCS curves all approximately increased with the increase in the porosity (corresponding to the grain size of sand) (Table 1); in other words, as the sand particle size decreased, the strength of the grouted sand increased, as confirmed by previous research results [22,23]. Zebovitz, Krizek [24] reported that this phenomenon occurs because the number of grain-to-grain contacts per unit volume of sand increases as the gradation of sand becomes finer or as the specific surfaces of the sand become larger; therefore, it is reasonable that the finer sand would exhibit higher strength than the coarser sand. Moreover, because of the presence of initial water in the specimen, the decrease in the UCS of grouted sand was also obviously observed. For example, the UCS of the small-grain grouted specimen without initial water (corresponding to the porosity of 40, see Figure 5) decreased from 12.83 MPa to 7.19 MPa (the UCS value of the small-grain grouted specimen containing initial water corresponding to the porosity of 37, see Figure 5) at the age of 28 days, a reduction of 44% compared to a reduction of 38% in a specimen of medium grain size and a reduction of 33% in a specimen of large grain size.

Figures 4b and 5b show the relationships of $E-t$ and $E-\phi$, respectively, where E is calculated as the average slope in the elastic deformation stage of the stress–strain curve. Overall, the average values of E appeared to be increasing with the increase in curing time and grain size (porosity), and this was similar to those of the UCS. For the grouted sand specimens with the same grain size, the average values of E in the specimens not containing the initial water were found to be significantly higher than those with the initial water. For example, they increased by approximately 66%, 55% and 57% after 28 days of curing in the specimens with small, medium, and large grain size, respectively, further demonstrating the adverse impact of initial water contained in sand on the mechanical behaviors of grouted sand.

The average values of peak axial strains of grouted specimens ranging from 3% to 6% are shown in Figure 4c. These results illustrated that the peak strains of different specimens were almost unchanged after 14 days of curing, revealing that the deformation characteristics of grouted specimens tended to be stable with the increase of curing time.

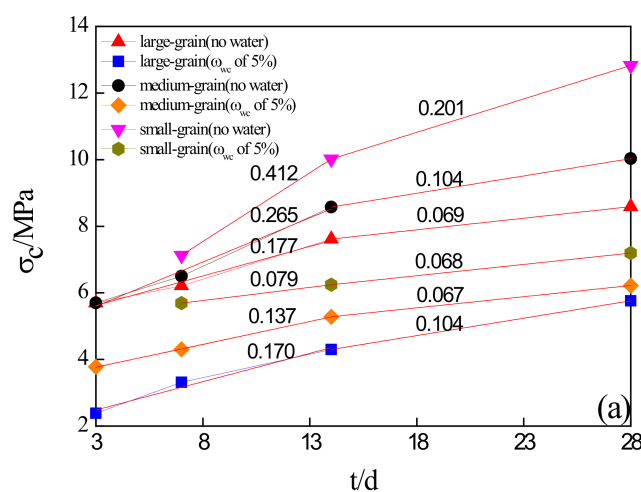


Figure 4. Cont.

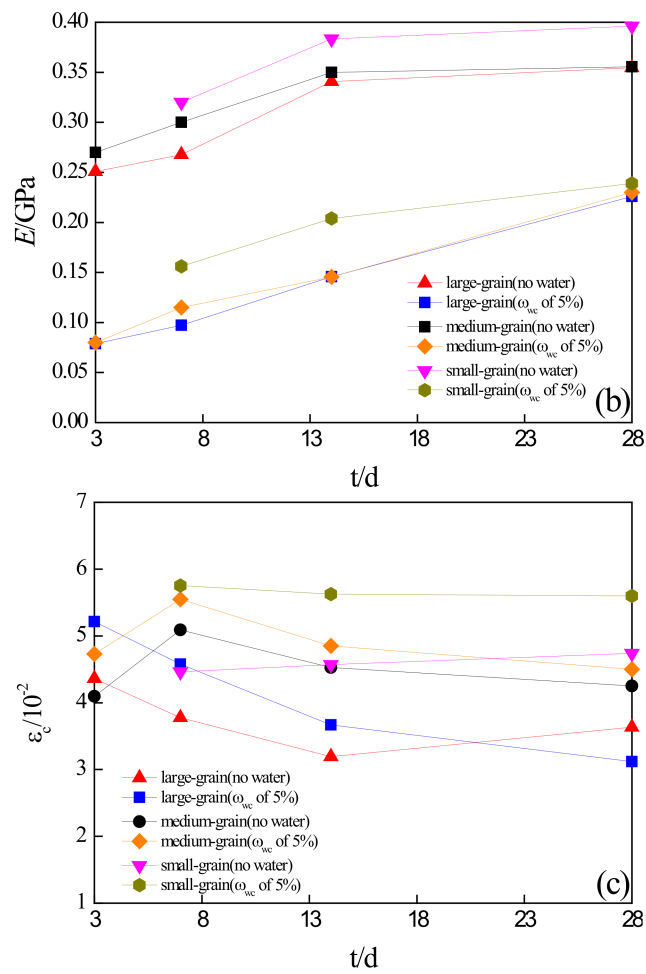


Figure 4. Different average values of mechanical parameters versus curing time. (a) σ_c , (b) E , (c) ϵ_c .

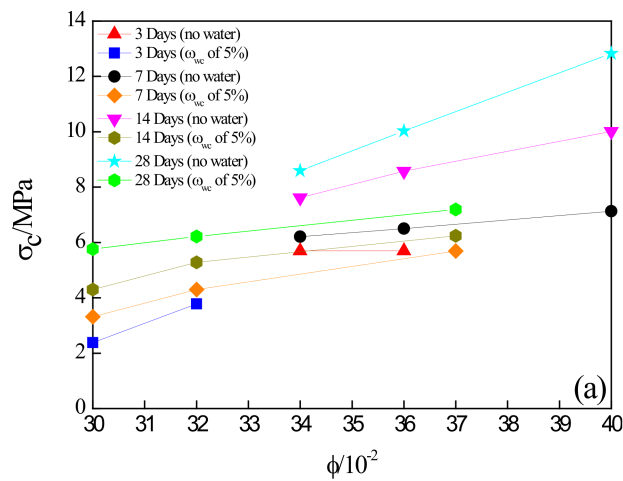


Figure 5. Cont.

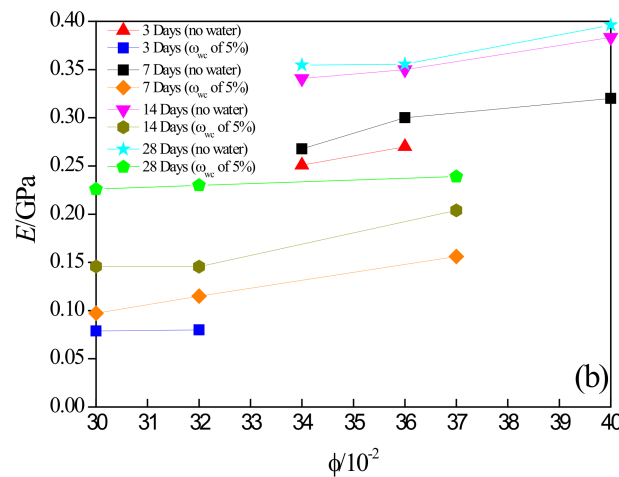


Figure 5. Different average values of mechanical parameters versus initial porosity. (a) σ_c , (b) E .

Table 3. Average values of mechanical parameters of grouted sand specimens.

Sand Types	ω_{wc} (%)	UCS (MPa)				E (GPa)					$\epsilon_c (\times 10^{-2})$					ϕ	
		3 d	7 d	14 d	28 d	σ	3 d	7 d	14 d	28 d	σ	3 d	7 d	14 d	28 d		σ
Large	0	5.70	6.21	7.62	8.59	1.34–3.12	0.25	0.27	0.34	0.35	0.14–0.29	4.36	3.78	3.19	3.63	0.04–0.09	34
	5	2.38	3.31	4.30	5.76	1.21–2.45	0.08	0.10	0.15	0.23	0.21–0.35	5.22	4.58	3.67	3.12	0.05–0.10	30
Medium	0	5.70	6.50	8.58	10.03	0.94–3.57	0.27	0.30	0.35	0.36	0.32–0.37	4.10	5.09	4.53	4.25	0.08–0.13	36
	5	3.78	4.30	5.28	6.22	0.89–2.63	0.08	0.11	0.15	0.23	0.19–0.54	4.73	5.55	4.85	4.5	0.03–0.05	32
Small	0	-	7.12	10.02	12.83	1.14–3.01	-	0.32	0.38	0.40	0.27–0.51	-	4.46	4.57	4.74	0.11–0.14	40
	5	-	5.69	6.24	7.19	1.25–1.85	-	0.16	0.20	0.24	0.38–0.43	-	5.75	5.62	5.60	0.09–0.15	37

Note: ω_{wc} refers water content of initial sand (before grouting); d represents days; σ means standard deviation; and ϕ represents porosity. For instance, UCS (E , ϵ_c) for 3 d means the average values of uniaxial compressive strength (elasticity modulus, peak axial strain) of the grouted sand specimens after 3 days of curing.

3.2. Microstructure Characteristics

According to Figure 6, which shows the SEM images of sections in grouted specimens (three pieces of specimens chosen with 28 days of curing), the preparation of SEM samples generally includes the following steps: determining the sampling site from the grouted samples, and then obtaining the SEM samples by thin section identification method. The abovementioned macroscopic mechanical results of the grouted sand (the finer the particle size of sand, the greater was the UCS of the grouted sand) can be explained from a microscopic perspective to a certain extent. For example, according to the magnified surfaces in the scale of 1:500 displayed in Figure 6(a₁–c₁), the finer the particle size of sand, the thicker and denser was the grout filling layer. In more detail, compared to the small-grain specimen magnified at the scale of 1:5000 (Figure 6(c₂)), micro-cracks that were not completely filled by UF grouts were found in the large- and medium-grain specimens because of the larger grain size of the sand, as shown in Figure 6(a₂,b₂). Moreover, referring to Figure 6(c₂), finer sand clearly possessed desirable filling performance because the UF grouts filled almost all of the voids and cracks between grains in many section surfaces; this observation was consistent with the observation results of other finer sand specimens after 7 and 14 days of curing. However, at present, it is difficult to draw reliable observations from qualitative SEM images. Therefore, the microstructural characteristics of grouted sand should be investigated and quantified in future research. Moreover, a study on the presence of such micro-cracks occurring in the grouted large-grain and medium-grain sand is needed in the next work because a dissipative phenomenon is associated to them [25–27]. Sometimes this dissipative behavior can be as a desired mechanical property, such as in absorbing seismic excitations, provided that it does not lower the resistance too much.

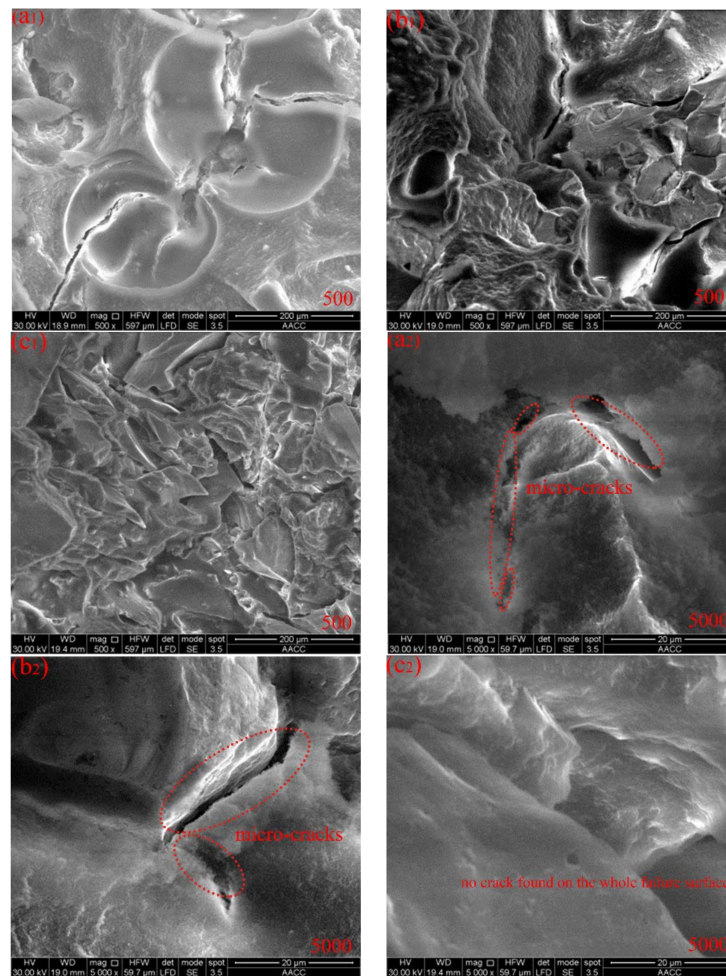


Figure 6. Representative SEM images (the magnifications are $500\times$ (set 1) and $5000\times$ (set 2)) of section surfaces in grouted sand specimens after 28 days of curing: (a) large-grain sand; (b) medium-grain sand; (c) small-grain sand.

4. Discussion

From the representative axial stress–strain curves shown in Figure 3, the ductile behaviors of various grouted sand specimens under uniaxial compression is analyzed below.

The stress–strain curves are divided into four stages: compaction stage, elastic deformation stage, yield stage, and post-peak stage. It was noticed that at the post-peak stage for all tested sand specimens, no obvious instant drop (brittle failures) occurred for the curves, demonstrating that the grouted sand specimen had the expected ductility with deformation up to a larger strain of approximately 7%, where the ultimate failure was observed; this property is advantageous to the delay of structural damage when disasters occur [28]. From the macroscopic and microscopic observations, the strong adhesion between the UF grouts and sand particles was found to essentially improve the mechanical and deformation characteristics of the grouted sand.

5. Conclusions

The finer grouted specimens were found to achieve higher strength, whereas the presence of initial water had a negative impact on the mechanical behaviors compared with the absence of water. These results are complemented and verified by the study of the microstructure through SEM, demonstrating that the grouts adhered better to the grains in the finer sand by almost filling all the cracks. Through the above study, the following conclusions can be drawn:

- (1) The gel time, concretion rate, and mechanical and rheological properties of the improved chemical grouts (UF-OA grouts) with various volume ratios of A and B were investigated to obtain a suitable ratio (A:B of 7) in the grouts used in this study.
- (2) With the increase in the grain size of the sand and the existence of initial water contained in sand, the values of the strength (UCS) and elastic moduli (E) for most of the grouted sand specimens decreased distinctly. Moreover, with the increase in the curing time, the UCS and E presented an increasing trend, and the mechanical behaviors of grouted sand after 14 days of curing were significantly improved. Moreover, the peak strains for the grouted specimens were found to remain constant with the increase of curing time after 14 days of curing.
- (3) The microstructural characteristics indicate that the finer grouted sand was found to achieve higher mechanical strength via the better filling performance.
- (4) Most of the grouted sand specimens under uniaxial compression at curing times of 3, 7, 14 and 28 days revealed desirable ductile failure characteristics.

Acknowledgments: The research described in this paper was financially supported by the National Natural Science Foundation of China (Grant Nos. 51704280 and 51574223), and the China Postdoctoral Science Foundation (Grant No. 2017T100420). The fourth author (Dan Ma) would like to thank the financial supported by State Key Laboratory for Geomechanics and Deep Underground Engineering, China University of Mining & Technology (SKLGDUEK1805) and Research Fund of State Key Laboratory of Coal Resources and Safe Mining, CUMT (SKLCRSM18KF024).

Author Contributions: Yuhao Jin, Lijun Han, Qingbin Meng and Guansheng Han conceived and designed the experiments; Yuhao Jin and Guansheng Han performed the experiments; Yuhao Jin and Dan Ma analyzed the data; Furong Gao and Shuai Wang contributed analysis tools; Yuhao Jin and Guansheng Han wrote the paper.

Conflicts of Interest: The authors declare no conflict of interest.

Notations

ω_{wc}	water content of initial sand (before grouting)
σ	standard deviation
φ	porosity
UF-OA	urea formaldehyde resin mixed with oxalate curing agent
σ_1	axial stress (MPa)
ε_1	axial strain (10^{-2})
UCS (σ_c)	uniaxial compressive strength (MPa)
E	elasticity modulus of grouted sand (GPa)
ε_c	peak axial strain (10^{-2})
t	curing time
SEM	scanning electron microscope

References

1. Liu, R.; Li, B.; Jiang, Y. A fractal model based on a new governing equation of fluid flow in fractures for characterizing hydraulic properties of rock fracture networks. *Comput. Geotech.* **2016**, *75*, 57–68. [[CrossRef](#)]
2. Liu, R.; Jiang, Y.; Li, B.; Wang, X. A fractal model for characterizing fluid flow in fractured rock masses based on randomly distributed rock fracture networks. *Comput. Geotech.* **2015**, *65*, 45–55. [[CrossRef](#)]
3. Huang, N.; Jiang, Y.; Li, B.; Liu, R. A numerical method for simulating fluid flow through 3-D fracture networks. *J. Nat. Gas Sci. Eng.* **2016**, *33*, 1271–1281. [[CrossRef](#)]
4. Liu, R.; Li, B.; Jiang, Y. Critical hydraulic gradient for nonlinear flow through rock fracture networks: The roles of aperture, surface roughness, and number of intersections. *Adv. Water Resour.* **2016**, *88*, 53–65. [[CrossRef](#)]
5. Avci, E. Performance of Novel Chemical Grout in Treating Sands. *J. Mater. Civ. Eng.* **2017**, *29*. [[CrossRef](#)]
6. Avci, E.; Mollamahmutoglu, M. UCS Properties of Superfine Cement–Grouted Sand. *J. Mater. Civ. Eng.* **2016**, *28*. [[CrossRef](#)]

7. Mohammed, M.H.; Pusch, R.; Knutsson, S.; Hellström, G. Rheological Properties of Cement-Based Grouts Determined by Different Techniques. *Engineering* **2016**, *6*, 217–229. [[CrossRef](#)]
8. Tan, O.; Gungormus, G.; Zaimoglu, A.S. Effect of Bentonite, Fly Ash and Silica Fume cement injections on uniaxial compressive strength of granular bases. *KSCE J. Civ. Eng.* **2014**, *18*, 1650–1654. [[CrossRef](#)]
9. Bras, A.; Gião, R.; Lúcio, V.; Chastre, C. Development of an injectable grout for concrete repair and strengthening. *Cem. Concr. Comp.* **2013**, *37*, 185–195. [[CrossRef](#)]
10. Anagnostopoulos, C.A.; Papaliangas, T.; Manolopoulou, S.; Dimopoulos, T. Physical and mechanical properties of chemically grouted sand. *Tunnell. Undergr. Space Technol.* **2011**, *26*, 718–724. [[CrossRef](#)]
11. Xing, H.G.; Dang, Y.H.; Yang, X.G.; Zhou, J.W. Experimental study of physical and mechanical properties of chemically grouted sand and gravel. *Sens. Transducers* **2014**, *165*, 164–169.
12. Porcino, D.; Ghionna, V.N.; Granata, R.; Marciandò, V. Laboratory determination of mechanical and hydraulic properties of chemically grouted sands. *Geomech. Geoeng.* **2015**, *11*, 164–175. [[CrossRef](#)]
13. Dayakar, P.; Raman, K.V.; Raju, K.V.B. *Study on Permeation Grouting Using Cement Grout in Sandy Soil*; Abzena: Cambridge, UK, 2012; Volume 4, pp. 5–10.
14. Alaa, A.; Vipulanandan, C. Cohesive and Adhesive Properties of Silicate Grout on Grouted-Sand Behavior. *J. Geotechn. Geoenviron. Eng.* **1998**, *124*, 38–44.
15. Delfosse-Ribay, E.; Djeran-Maigre, I.; Cabrillac, R.; Gouvenot, D. Factors Affecting the Creep Behavior of Grouted Sand. *J. Geotech. Geoenviron. Eng.* **2006**, *132*, 488–500. [[CrossRef](#)]
16. Gonzalez, H.A.; Vipulanandan, C. Behavior of a Sodium Silicate Grouted Sand. In Proceedings of the Geo-Denver, Denver, CO, USA, 18–21 February 2007; pp. 1–10.
17. Hassanlourad, M.; Salehzadeh, H.; Shahnazari, H. Undrained triaxial shear behavior of grouted carbonate sands. *Int. J. Civ. Eng.* **2011**, *9*, 307–314.
18. Porcino, D.; Marciandò, V.; Granata, R. Static and dynamic properties of a lightly cemented silicate-grouted sand. *Can. Geotech. J.* **2011**, *49*, 1117–1133. [[CrossRef](#)]
19. Park, B. Properties of Urea-Formaldehyde Resin Adhesives with Different Formaldehyde to Urea Mole Ratios. *J. Adhes.* **2015**, *91*, 677–700.
20. Cao, X.X.; Zhang, Y.H.; Zhu, L.B.; Tan, H.Y.; Ji-You, G.U. Study on the Curing Characteristics and Synthesis Process of Modified Urea-formaldehyde Resin with Low Formaldehyde Release. In Proceedings of the 3rd International Conference and Exhibition on Biopolymers & Bioplastics, San Antonio, TX, USA, 12–14 September 2016.
21. Yang, S.Q.; Liu, X.R.; Jing, H.W. Experimental investigation on fracture coalescence behavior of red sandstone containing two unparallel fissures under uniaxial compression. *Int. J. Rock Mech. Min. Sci.* **2013**, *63*, 82–92. [[CrossRef](#)]
22. Schwarz, L.G.; Krizek, R.J. Hydrocarbon Residuals and Containment in Microfine Cement Grouted Sand. *J. Mater. Civ. Eng.* **2006**, *18*, 214–228. [[CrossRef](#)]
23. Markou, I.N.; Droudakis, A.I. Factors Affecting Engineering Properties of Microfine Cement Grouted Sands. *Geotech. Geol. Eng.* **2013**, *31*, 1041–1058. [[CrossRef](#)]
24. Zebovitz, S.; Krizek, R.J.; Atmatzidis, D.K. Injection of Fine Sands with Very Fine Cement Grout. *J. Geotech. Eng.* **1989**, *115*, 1717–1733. [[CrossRef](#)]
25. Scerrato, D.; Giorgio, I.; Della Corte, A.; Madeo, A.; Limam, A. A micro-structural model for dissipation phenomena in the concrete. *Int. J. Numer. Anal. Methods Geomech.* **2015**, *39*, 2037–2052. [[CrossRef](#)]
26. Giorgio, I.; Scerrato, D. Multi-scale concrete model with rate-dependent internal friction. *Eur. J. Environ. Civ. Eng.* **2016**, *21*, 821–839. [[CrossRef](#)]
27. Contrafatto, L.; Cuomo, M.; Fazio, F. An enriched finite element for crack opening and rebar slip in reinforced concrete members. *Int. J. Fract.* **2012**, *178*, 33–50. [[CrossRef](#)]
28. Christensen, R.M. Exploration of ductile, brittle failure characteristics through a two-parameter yield/failure criterion. *Mater. Sci. Eng. A* **2005**, *394*, 417–424. [[CrossRef](#)]

